Materials Transactions, Vol. 60, No. 7 (2019) pp. 1159 to 1167
Special Issue on Severe Plastic Deformation for Nanomaterials with Advanced Functionality
©2019 The Japan Institute of Metals and Materials

Room Temperature Superplaticity in Fine/Ultrafine Grained Materials Subjected to Severe Plastic Deformation

M. Demirtas[1] and G. Purcek[2,*]

[1]*Department of Mechanical Engineering, Recep Tayyip Erdogan University, Rize 53100, Turkey*
[2]*Department of Mechanical Engineering, Karadeniz Technical University, Trabzon 61080, Turkey*

Achieving superplasticity at high temperatures and at very low strain rates is considered to be the most important disadvange of superplastic forming processes. Therefore, it is crucial to achieve superplastic behavior at low temperatures and high strain rates. To do so, it is well known that, high amount of grain refinement in the superplastic material is required. Very recent advances in severe plastic deformation (SPD) techniques based on imposing very high strains to the material provide abnormal grain refinement, and ultrafine-grained (UFG) microstructures can be achived in metallic materials by this manner. Formation of UFG microstructures via SPD methods like equal channel angular pressing (ECAP), high pressure torsion (HPT) and friction stir processing (FSP) bring about superplastic behavior in some classes of alloys even at room temperature (RT) as an extreme example of low temperature superplasticity. This paper overviews the studies aiming to investigate the RT superplasticity in some specific metals and alloys after UFG formation by SPD methods. UFG formation or nanostructuring of the materials by SPD to attain RT superplasticity were analyzed in detail. Also, the parameters affecting the RT superplasticity in different classes of materials and superplastic deformation mechanisms operated at RT superplasticity were explained. [doi:10.2320/matertrans.MF201922]

(Received February 15, 2019; Accepted March 7, 2019; Published May 31, 2019)

Keywords: *severe plastic deformation, ultrafine-grained materials, superplasticity, room temperature superplasticity*

1. Introduction

The ductility of conventional engineering materials can be increased to the required levels for manufacturing by thermal and/or thermomechanical processes or by addition of alloying elements. On the other hand, it is necessary to improve the ductility of these materials further, especially when it is desired to produce much more complex-shaped parts in space, aerospace and automotive industry as well as architecture. Previous studies have shown that some polycrystalline materials exhibit extremely high neck-free tensile elongations if a number of microstructural and experimental requirements are fulfilled.[1,2] This behavior of materials is called as superplasticity, and superplastic forming technology based on this phenomena makes possible to produce complex-shaped parts from such materials for some engineering applications.[3]

As stated above, superplastic behavior in metals is controlled by some microstructural and process parameters. These main parameters are deformation temperature, grain size of the material and strain rate at which the material is tensioned. First, the material must be deformed at high temperature regimes above 0.5 Tm (Tm is the absolute melting point of the material). Second, the materials should have at least a fine-grained (FG) microstructure. Although the required grain size for superplasticity depends on the material, it is stated in superplasticity related studies that the grain size should generally be lower than 10 μm in order to obtain superplastic behavior in metals.[1,4] Third, the deformation should be performed at low strain rates ranging between $1 \times 10^{-5}\,s^{-1}$ and $1 \times 10^{-3}\,s^{-1}$ for giving enough time to diffusional deformation mechanism leading to high elongation.

Achieving superplasticity at high temperatures and at very low strain rates, on the other hand, is considered to be the most important disadvantage of superplastic forming.[5] In particular, obtaining superplastic behavior at low strain rates means that each part can be produced in approx. 20–30 min in the production methods using this technology,[6,7] which also increases the manufacturing cost. Therefore, it is important to achieve superplastic behavior at relatively high strain rates so that superplastic forming technology can be used more widely and economically. Consequently, it has been gained special attention to achieve superplastic behavior at low temperature and high strain rates in order to enhance the applications of superplasticity and to reduce the cost of superplastic forming.

High temperature plastic flow, including superplasticity, can be expressed by the constitutive creep equation in the following form:[8]

$$\dot{\varepsilon} = \frac{ADGb}{kT}\left(\frac{b}{d}\right)^{p}\left(\frac{\sigma}{G}\right)^{n} \tag{1}$$

where $\dot{\varepsilon}$ is the strain rate, A is a dimensionless constant, D is the diffusion coefficient ($= D_o\, exp(-\frac{Q}{RT})$, where Q is the activation energy, D_o is a frequency factor and R is the gas constant and T is the absolute temperature) G is the shear modulus, b is the burgers vector, σ is the flow stress, k is the Boltzmann's constant, d is the grain size, n is the stress exponent and p is the inverse gran size exponents. From eq. (1), it is clear that any decrease in grain size of the superplastic material increases the strain rate and decreases the temperature at which superplastic behavior is observed.[1,9] With evidence that the grain size has such an effect on the temperature in superplastic behavior, studies on superplasticity have gained a new dimension and a new field of study has been created under the name of low temperature superplasticity. As an extreme example of this, it was shown that it was possible to obtain superplastic behavior even at room temperature (RT) by ultrafine-grain (UFG) formation in the microstructure of some superplastic or potentially superplastic materials.

*Corresponding author, E-mail: purcek@ktu.edu.tr

Considering the above mentioned issues, it is clear that grain refinement is the key point for achieving superplastic elongations at low temperature (particularly at RT) and high strain rates. Grain refinement has also some other benefits in superplasticity and superplastic forming. When the strain rate and temperature are kept constant, it is possible to achieve higher superplastic elongation by reducing grain size of the material. The grain size of the superplastic materials also has a significant effect on its yield strength. Hall-Petch relation becomes invalid at ambient temperatures below a critical grain size where transition from the usual deformation to superplastic deformation occurs.[10–12] Therefore, decreasing grain size also decreases the strength of the superplastic materials due to the easier grain boundary sliding (GBS) at more grain boundary areas. This effect was also reported in same special materials exhibiting superplasticity even at RT which corresponds to higher than ~0.40 Tm of these materials.[10,12] Lower flow stress brings about lower manufacturing force requirement during the superplastic forming and results in energy savings. Therefore, formation of UFG microstructures in superplastic materials have become a great interest amongst the scientists and researchers who study on this area.

It is known that conventional plastic deformation techniques like rolling, forging and extrusion provide some grain refinement in metals. However, it is difficult to achieve grain refinement down to submicron level (UFG formation) using these conventional methods. Because, extremely high strain should be imposed to the metallic materials to convert a coarse-grained (CG) or FG microstructure into the UFG ones.[13] Recently, some novel grain refinement techniques based on imposing very high strains to the material by severe plastic deformation (SPD) have been developed. It has been shown that grain size of the metallic materials can be decreased down to micron or sub-micron levels using the SPD methods like equal channel angular pressing (ECAP), high pressure torsion (HPT) and friction stir processing (FSP). These methods have been used efficiently to attain significant grain refinement to achieve room temperature superplasticity in some classes of materials.

In view of above, the present study overviews the available studies aiming to investigate the room temperature superplasticity in a range of metals and alloys after SPD processing. Specifically, this report has several objectives. The following section describes nanostructuring of the materials by SPD to attain room temperature superplasticity. In the last part, the parameters affecting room temperature superplasticity in different classes of materials and superplastic deformation mechanisms operated at room temperature were explained.

2. Nanostructuring of Materials via SPD for Room Temperature Superplasticity

As stated above, grain refinement brings about superplasticity at lower temperatures according to eq. (1), and most of the studies aiming to achieve superplastic behavior at room temperature are based on this principle. However, grain refinement alone is not sufficient to attain RT superplasticity. In addition, material should also has low melting point so that grain refinement leads to GBS as the main superplastic deformation mechanism at RT. Based on these principles, RT superplasticity has been reported in some low melting-point Zn–Al alloys including eutectoid Zn–22Al,[14–22] eutectic Zn–5Al[23] and quasi-single phase Zn–Al alloys having Al content up to 1.1%[10] by means of significant grain refinement via SPD methods. Table 1 summarizes the reported data on RT superplasticity in these alloys with used grain refinement techniques, achieved grain size (d) and recorded elongations (ε_f) for each reference. It is seen that eutectoid Zn–22Al alloy is the most commonly studied one to achieve RT superplasticity, and ECAP has been successfully utilized for grain refinement to attain UFG microstructure in this alloy. In these studies, effects of ECAP temperature, phase regime where ECAP is applied to the alloy and number of ECAP passes on the final microstructure were analyzed. Tanaka *et al.*[14,15] investigated the effect of performing ECAP during the phase transformation on the microstructure of Zn–22Al alloy. To do so, 4 passes ECAP were conducted at RT immediately after quenching process (during the phase transformation). Knowing that phase transition from single phase to two phases is fully completed within 20 min in the microstrucutre of the quenched Zn–22Al,[24] 8 passes ECAP were also applied to the alloy at RT two hours later from the quenching for comparison. It was shown that performing ECAP during the phase transformation resulted in almost the same microstructure with that of performed after transformation is completed. Both process brought about an equiaxed microstructure having mostly high angle grain boundaries (HAGBs) and ~300 nm grain size. Regarding that pass number in the former process is half of the latter one, it was concluded that performing ECAP during the phase transformation is more efficient in grain refinement in Zn–22Al alloy. In the same study, it was examined also the effect of ECAP temperature on the achieved microstructure. 8 passes ECAP performed at 100°C after phase transition resulted in 600 nm grain sized microstructure which is coarser than that of performed at RT up to the same passes. It was demonstrated that decreasing ECAP temperature results in more homogeneous microstructure with finer grain size. ECAP temperature was futher increased by Huang and Langdon,[16] and they applied 8 passes ECAP to the alloy at a high temperature of 200°C. This process brought about a microstructure having 1300 nm grain size which is larger than that achieved after ECAP processing at lower temperatures. Effect of ECAP temperature on the final microstructure was also evaluated by Yang *et al.*[17] They processed the alloy via ECAP up to 8 passes at different temperatures of −10°C, RT and 50°C. Similar to the results published in Refs. 14, 15, decreasing ECAP temperature also decreased the final grain size of the alloy, and grain sizes after ECAP processing at −10°C, RT and 50°C were determined to be 300 nm, 500 nm, and 800 nm, respectively. More recently, Demirtas *et al.*[18,19] investigated the effect of two-step ECAP on the microstructure of the Zn–22Al alloy. They processed the alloy at different temperatures and phase regimes. In the first step, they subjected the alloy to 4 passes ECAP at 100°C and 250°C where the alloy has dual phase microstructure and at 350°C corresponding to single-phase region above eutectoid temperature of 275°C to evaluate the effects of ECAP

Table 1 A list of UFG materials processed by various SPD methods and showed room temperature superplasticity.

Alloy	*Processing*	d_f, (*nm*)	*m*	$\dot{\varepsilon}$ (s^{-1})	*Max.*ε_f (%)	*Ref.*
Zn-22Al	4 passes ECAP at RT during phase transformation	350	0.25	1×10^{-2}	240	14, 15
	8 passes ECAP at RT after phase transformation	300				
	8 passes ECAP at 100 ºC after phase transformation	600				
	8 passes ECAP at 200 ºC	1300		1×10^{-4}	250	16
	8 passes ECAP at -10 ºC	300	0.4	1×10^{-2}	180	17
	8 passes ECAP at RT	500				
	8 passes ECAP at 50 ºC	800	0.6	1×10^{-2}	250	
	4 passes ECAP at 100 ºC	500		1×10^{-2}	315	18
	4 passes ECAP at 250 ºC	1000		1×10^{-3}	195	
	4 passes ECAP at 350 ºC	250		1×10^{-3}	110	
	4 passes ECAP at 100 ºC + 4 passes ECAP at RT	400				19
	4 passes ECAP at 250 ºC + 4 passes ECAP at RT	700				
	4 passes ECAP at 350 ºC + 4 passes ECAP at RT	200	0.30	5×10^{-2}	400	
	8 passes ECAP at RT	550	0.35	4×10^{-3}	335	20
	4 passes ECAP at 200 ºC	800				21
	8 passes ECAP at 200 ºC	700				
	20 passes ECAP at 200 ºC	900				
	24 passes ECAP at 200 ºC	900		1×10^{-3}	260	
	FSP at RT	<1000	0.25	1×10^{-2}	160	22
Zn-5Al	8 Passes ECAP at RT	540	0.25	1×10^{-3}	520	23
Zn-0.3Al	Rolling + 6 Passes ECAP at RT	2000	0.31	1×10^{-4}	1000	10
Al-30Zn	200 turns HPT	280	0.41	5.5×10^{-5}	480	46
Mg-8Li	200 turns HPT	240	0.37	1×10^{-3}	440	47

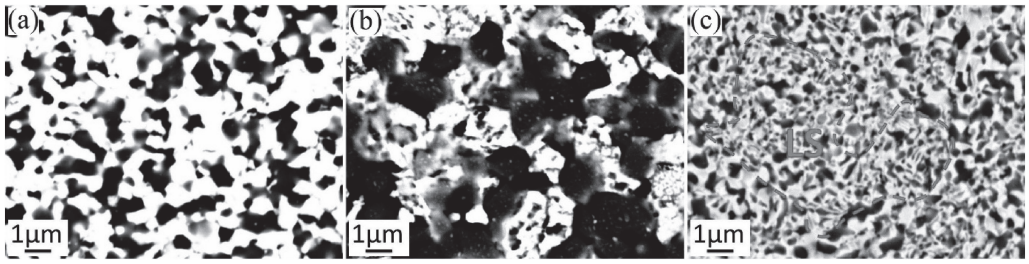


Fig. 1 SEM images showing the microstructure of the Zn–22Al alloy processed via ECAP at different temperatures of: (a) 100°C, (b) 250°C and (c) 350°C.[18)]

temperature and phase region on the achieved microstructure. Some representative SEM images showing the microstructure of the alloy processed via ECAP at different temperatures and phase regions are given in Fig. 1.[18)] Processing of the alloy in two-phase region below the eutectoid temperature brought about similar results with the previous studies;[14,15,17)] more refined microstructures were observed with decreasing process temperature. Grain sizes were measured as 500 nm and 1000 nm after ECAP processes performed at 100°C and 250°C, respectively (Fig. 1(a) and (b)). On the other hand, application of ECAP process at 250°C resulted in formation of Zn-rich η-phase particles in Al-rich α-phases (similarly, α-phase particles in η-phases) (Fig. 1(b)) while the other process brought about a microstructure containig α- and η-phases seperated from each other clearly (Fig. 1(a) and (c)). This result was attributed to the mixing of two phases due to the high processing temperature of 250°C instead of grain refinement by division into smaller grains.

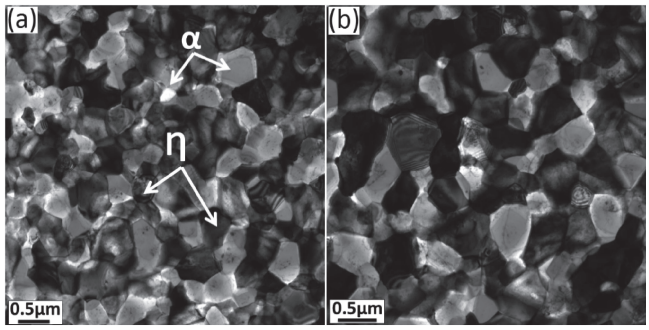


Fig. 2 TEM micrograph of Zn–22Al alloy processed via two-step ECAP (4 passes at 350°C + 4 passes at RT).[19)]

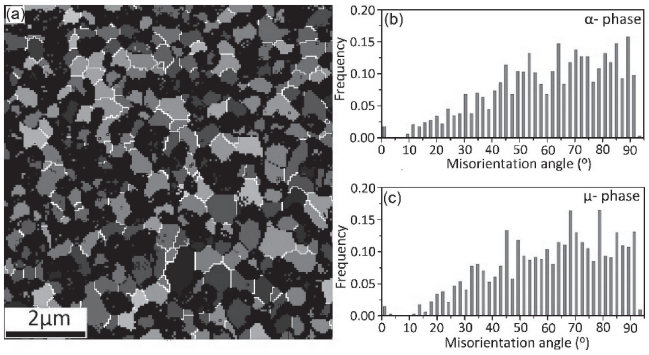


Fig. 3 (a) EBSD map and (b)–(c) histograms showing the grain boundary misorientation distributions of both Al-rich α- and Zn-rich η-phases of two-step processed Zn–22Al alloy.[19)]

Interestingly, increasing ECAP temperature to 350°C and processing the alloy in the single phase region brought about more refined microstructure with 250 nm grain size and with some lamellar structure (LS) coming from the casting stage of the alloy (Fig. 1(c)).[18)] Actually this result is not consistent with the well known information about the dependence of grain size on the ECAP temperature that the higher pressing temperatures result in larger grains.[25–30)] The unexpected result was attributed to the processing of the alloy at the single phase region and quenching the alloy after each subsequent ECAP pass. It was concluded that grain refinement effect of both ECAP and quenching was combined in this process since quenching of Zn–22Al alloy above the eutectoid temperature also resulted in some grain refinement.[24)] Thus, although the processing temperature was the highest one among all first step ECAP processes, this process resulted in the finest grain size. In the second step, they processed the alloy for four more passes applied to the billets at RT followed by first step ECAP performed at 100°C and 250°C and 350°C. It was demonstrated that the lamellar structure existed in the microstructure after 4 passes ECAP at 350°C was completely eliminated by four more passes at RT and this process brought about the lowest grain size of 200 nm (Fig. 2),[19)] which is also the lowest one reported in that alloy up to date. Processing the alloy via two-step ECAP brought about a microstructure where almost all of the grain boundaries separated from each other by high angle of misorientation (Fig. 3(b)–(c)) due to the accumulation of strain imposed during each ECAP pass.[31–37)] Besides, this process resulted in dislocation-free and equiaxed grains in the microstructure (Fig. 2). This result was attributed to the dynamic recrystallization occurred during the ECAP processing of the alloy at RT. Yang *et al.*[17)] also stated that dynamic recrystallization occurred during ECAP applied to the alloy at −10°C, RT and 50°C, and equiaxed grainy morphology was observed after these processes. Dynamic recrystallization/grain growth during ECAP processing of Zn–22Al alloy was reported in Ref. 20, too. Xia *et al.*[20)] homogenized and quenched the 10 μm grain-sized Zn–22Al alloy and then they processed it for 8 passes ECAP at RT. They reported that, ECAP decreased the grain size of the alloy to about 550 nm. It was stated in the same study that aging of quenched Zn–22Al alloy at RT for 72 hours brought about more refined microstructure as compared to the ECAP processed one. This result was attributed to strain-induced dynamic grain growth occurred during the ECAP processing of the alloy at RT corresponding to 0.43 Tm.

Effect of ECAP pass number on the microstrucure of Zn–22Al alloy was investigated by Kumar *et al.*[21)] They processed Zn–22Al alloy with an initial grain size of 1.8 μm at 200°C for various numbers of ECAP passes up to a maximum passes of 24. Processing the alloy via ECAP for four passes decreased the grain size to about 800 nm, and increasing the number of passes did not cause further grain refinement. Furthermore, a very small increase in grain size was observed in the alloy after large number of ECAP passes. It was stated that a slight increase in the grain size with increasing number of ECAP pass was not consistent with a proposed model for microstructural evolution in which increasing the imposed strain decreased the grain size[38)] by converting dislocation cells and sub-grain boundaries in to the HAGBs. This paradox between the imposed strain and achieved grain size was attributed to longer exposure of the alloy to the high ECAP temperature of 200°C.[21)]

Regarding the results available in the literature and summarized above, three main inferences can be made about the ECAP processing of Zn–22Al alloy to attain UFG microstructure required for room temperature superplasticity. First, it is beneficial to keep ECAP temperature as low as possible when the alloy was processed in a one-step ECAP process applied to the alloy in two phase regions (below the eutectoid temperature). Second, application of ECAP during the phase transformation and in the single phase region are more efficient in grain refinement. Third, processing the alloy via two-step ECAP where hot step was applied to the alloy in the single phase region above the eutectoid temperature of 275°C can be considered as the optimal processing route to achieve UFG microstructure with the finest grain size in that alloy.

Zn–22Al alloy was also processed by FSP as an another SPD method, and FSP refined the grain size of the alloy down to 1000 nm. It was also stated that the texture coming from the rolling stage of the initial material became random due to the FSP.[22)]

Eutectic Zn–5Al and quasi single phase Zn–0.3Al alloys are the other potential RT superplastic alloys in the binary Zn–Al system. Processing of Zn–5Al alloy via ECAP at RT up to eight passes eliminated its initial lamellar microstructure completely and brought about a unique bimodal

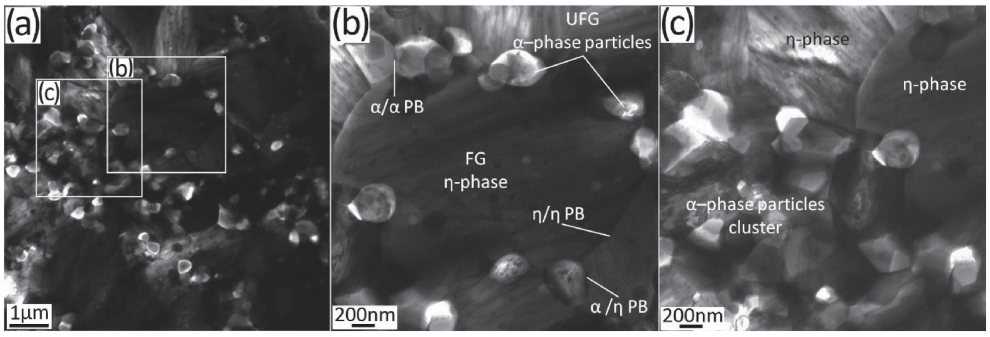


Fig. 4 TEM micrographs showing the bi-modal microstructure of Zn–5Al alloy processed via 8 passes ECAP at RT.[23)]

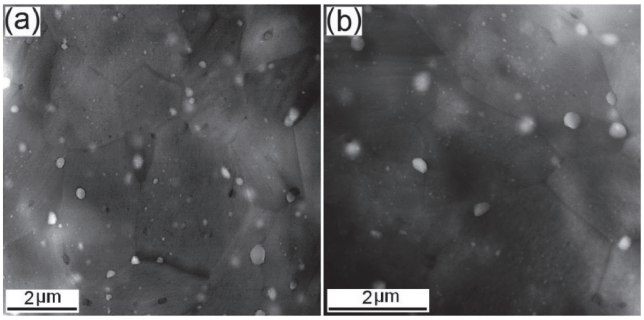


Fig. 5 TEM micrographs of 6 passes ECAP-processed Zn–0.3Al alloy: (a) flow plane and (b) transverse plane.[13)]

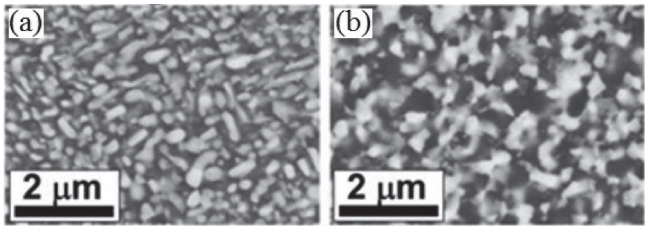


Fig. 6 SEM-BSE images showing the microstructure of (a) initial and (b) HPT-processed Al–30Zn alloy.[46)]

microstructure in the UFG regime with the equiaxed grains. α-phase grains decorated mostly at the relatively coarser η-phase grain boundaries (Fig. 4(a)–(c)). The mean grain sizes of the α- and η-phases were determined to be 110 nm and 540 nm, respectively.[23)] The morphologically unique structural formation was attributed to the microstructural transformation of the phases in the microstructure of the alloy during ECAP processing.[23)] ECAP was applied to Zn–0.3Al alloy by Demirtas *et al.*[13)] to refine the microstructure of the alloy. Two precautions were undertaken to avoid the fracture of the alloy during the ECAP processing due to the quite brittle behavior of the alloy in the quenched form. First, the alloy was hot rolled at 100°C with a reduction in thickness of 35% to provide more ductility prior to the ECAP processing.[39,40)] Second, the ECAP process was utilized using route-A where the ECAP sample is put to the channel in the same position in each pass. Application of six passes ECAP to the hot rolled alloy (initial grain size is about 5 μm) at RT decreased the grain size of the alloy down to 2000 nm. It was also shown that processing of the alloy via ECAP brought about equiaxed grain size in both flow and transverse planes of the alloy (Fig. 5(a)–(b)). It is well known that route-A results in elongated grains on the flow plane of the ECAP billet.[41–43)] Equiaxed grainy morphology on the flow plane of the Zn–0.3Al alloy processed through 6 passes ECAP using route-A was attributed to the dynamic recrystallization occurred during the ECAP process due to the low recrystallization temperature (-12°C)[44)] of the matrix phase of η.[45)] These results show that ECAP processing of Zn–5Al and Zn–0.3Al alloys resulted in dynamic recrystallization, as in the case of Zn–22Al alloy, regarding the dislocation-free microstructures with equiaxed grainy morphology observed in these alloys.

Regarding the eq. (1), Edalati *et al.*[46,47)] suggested that decreasing the temperature at which superplasticity is achieved is also possible by enhancing grain-boundary diffusion with modification of the chemical composition of the boundaries. As an evidence of this suggestion, they processed Al–30Zn[46)] and Mg–8Li[47)] alloys at RT via HPT with $N = 200$ cycles. It was demonstrated that HPT processing of Al–30Zn for 200 cycles did not cause significant grain refinement, even some grain growth was achieved during this process. Mean grain sizes were reported to be 210 nm and 280 nm for initial and HPT-processed Al–30Zn alloys, respectively (Fig. 6(a)–(b)).[46)] Mg–8Li was also processed by HPT to achieve room temperature superplasticity in this alloy.[47)] 2.2 μm grain-sized initial microstructure of the alloy refined and a UFG microstructure having 240 nm grain size was achieved after 200 HPT cycles.

3. Room Temperature Superplasticity in UFG Materials Processed by SPD

UFG formation in the above-mentioned alloys via SPD brought about RT superplasticity, and achieved elongations are given in Table 1. When these studies are carefully examined, it is seen that superplastic elongation of these alloys depends on some microstructural parameters like size and shape of the grains, homogeneity of the phase distribution throughout the microstructure and chemical composition of the phase/grain boundaries. In general, finer grain size resulted in higher superplastic elongation, as expected,[1–4)] due to the increment of the grain boundaries in a specific volume of microstructure.[48)] Since gage section dimensions of the tensile test sample affects the elongation to failure,[49,50)] it is not adequate to compare the results reported in different studies for the same alloy in Table 1.

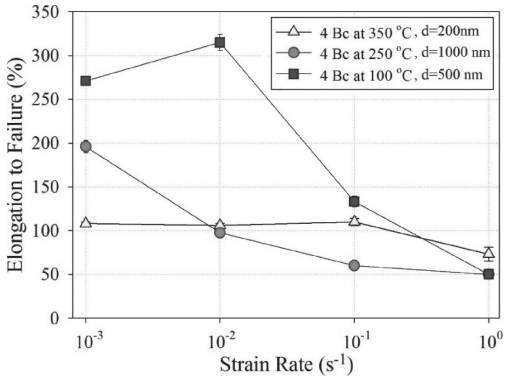


Fig. 7 The variation in elongation to failure with strain rate in ECAPed UFG Zn–22Al alloy having different grain sizes (d).[18)]

Therefore, evaluating the grain size and elongation values of each study within themselves is thought to be a more appropriate approach. Decreasing grain size from 1000 nm to 500 nm increased elongation from 195% to about 315%, respectively, in eutectoid Zn–22Al alloy.[18)] It was also stated in the same study that 250 nm grain sized microstructure resulted in a lower elongation to failure of 110% (Fig. 7). These results are not consistent with the well-known information about the dependence of elongation to failure on the grain size in superplastic materials.[1,11)] This paradox between the grain size and elongation to failure was attributed to the difficulty of accommodation of GBS by dislocation motion due to the lamellar structure still existed in the microstructure of the sample having the lowest grain size of 250 nm. It is now well established that GBS is accommodated by intragranular dislocation slip process to relief stress concentrations.[4)] It was demonstrated that lamellar structure prevented the dislocations climbing along the grain boundaries or gliding along the most favorable slip plane of the next grains. Thus, stress concentration occurred near the lamellar structure due to the dislocation pile-up and it caused nucleation of some microcracks.[18,51)] As the deformation continued, this microcracks attained large sizes and caused the premature failure. Similar result was also reported in Ref. 20. Formation of 250 nm grain sized microstructure with high aspect ratio of 2.6 brought about lower elongation than that of observed in an another sample having relatively coarser grains (550 nm) with exuiaxed morphology. It has been stated that the stress concentration at the grain boundaries of the elongated grains decreased the elongation to failure and resulted in lower elongation than the expected value regarding the grain size. Besides the grain size, these results show that shape of the grains also effect the total elongation in superplastic materials and equiaxed grainy morphology is more beneficial to achieve higher superplastic elongations.

It is clear from eq. (1) that any decrease in grain size increases the strain rate at which the maximum superplastic elongation is achieved. The reported results in RT superplasticity of UFG eutectoid Zn–22Al is well consistent with this theoretical model. Regarding two studies where the highest elongations were achieved at RT, decreasing grain size from 550 nm to about 200 nm increased the strain rate causing the maximum elongation from $4 \times 10^{-3}\,s^{-1}$ to $5 \times 10^{-2}\,s^{-1}$ (Fig. 8). This further grain refinement to 200 nm resulted in also the highest superplastic elongation of 400% observed in SPD processed Zn–22Al alloy at RT. It was shown that fracture in UFG Zn–22Al alloy resulted from the diffusion-controlled cavity growth.[52)] Therefore, achieving superplasticity at higher strain rates in UFG Zn–22Al alloy having 200 nm grain size resulted in the highest superplastic elongation of 400% due to the less time for initiation and growth of internal cavities causing premature failure.[53–56)] This significant increase in the superplastic elongation was also attributed to the agglomerate-free UFG microstructure of Zn–22Al alloy with equiaxed grain morphology and high angle of grain boundaries since these boundaries slide easily due to their high energy level.[57–60)]

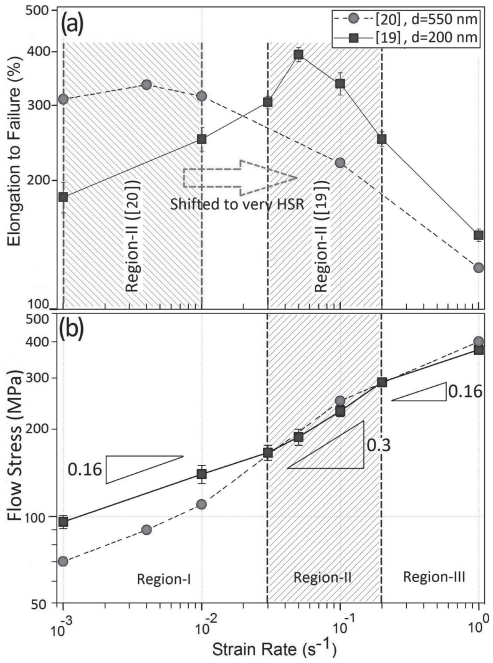


Fig. 8 Variation of elongation to failure and flow stress with strain rates in ECAPed UFG Zn–22Al alloy.[19,20)]

Microstructural homogeneity was stated to be another important parameter affecting the superplastic elongation. It was found that homogeneous distribution of α- and η-phases of Zn–Al superplastic alloy promoted elongation to failure and resulted in higher superplastic elongation in that alloy. It was shown that contribution of GBS to total elongation increased with decreasing the degree of agglomeration in the microstructure of Zn–22Al alloy.[61)] It was also shown that agglomeration of the phases in Zn–22Al prevented to achieve an increase in the elongation to failure although the grain size decreased.[62)] Different phase boundaries in Zn–Al alloys have different sliding characteristics. While η/η and η/α phase boundaries are the most favorable ones for grain boundary sliding, α/α phase (or grain) boundaries do not slide easily.[63–66)] Agglomeration of α- and η-phases in the microstructure leads to presence of large number of α/α phase boundaries and causes less grain boundary sliding. It was found that the homogeneous distribution of the phases in the agglomerate-free microstructure of Zn–22Al alloy formed after two-step ECAP processing resulted in the highest superplastic elongation in this alloy at RT.[19)]

Besides the agglomeration, phase composition also effects the proportion of each phase boundaries in the Zn–Al alloys. Decreasing Al content decreases also the formation of α/α phase boundaries, which is favorable for high superplastic elongation in these alloys. This effect can be clearly seen in the TEM micrographs of Zn–Al alloys given in Figs. 2, 4 and 5. While almost all of the grain boundaries were in the form of η/η in the Zn–0.3Al, the highest α/α boundary formation were observed in Zn–22Al alloy. Thus, although Zn–0.3Al had the largest grain size among all superplastic or potentially superplastic Zn–Al alloys, the highest superplastic elongation was achieved in this alloy due to the effective grain boundary sliding mainly in-between η/η phase boundaries. The lowest superplastic elongation was reported in Zn–22Al alloy having the smallest grain size, and Zn–5Al alloy showed moderate superplastic elongation. These results show that, phase composition also has a significant effect on the RT superplastic elongations in metals and alloys besides the grain size and shape of the grains.

Regarding the RT superplasticity of UFG Zn–Al alloys, eutectoid, eutectic and quasi-single phase alloys have been generally studied. However, Edalati *et al.*[46] showed that RT superplasticity can also be achieved in Al–30Zn alloy having high fraction of α/α phase boundaries in the microstructure. As stated above, processing of this alloy via HPT up to 200 turns did not cause grain refinement. However, HPT-processed alloy exhibited superplastic elongation of 480% at RT (Table 1) while initial homogenized sample with smaller grain size showed poor plasticity with lower than 50% elongation. Thus, it may be said that formation of UFG microstructure is not enough alone for achieving superplasticity especially in Al–Zn alloys having high fraction of α/α phase boundaries, as validated by some earlier studies where RT superplasticity was not be able to observed in UFG Al–Zn alloys.[67,68] It was demonstrated in Ref. 46 that processing of Al–30Zn for high HPT cycles accelerated the segregation of Zn atoms at the α/α grain boundaries and resulted in high Zn concentration at these boundaries (Fig. 9) as in the case of Refs. 67, 69 where Al–Zn alloys were processed by HPT. Formation of a few layers of Zn atoms at the α/α boundaries enhanced the grain-boundary diffusion in these boundaries and made them favorable for GBS. Thus, deformation mechanism changed from dislocation activity to GBS after HPT via enhanced diffusion at the α/α boundaries which brought about high superplastic elongation in Al–30Zn alloy even at RT corresponds to 0.36 Tm of that alloy. Similar result was also reported in Mg–8Li alloy processed via HPT up to 200 turns.[47] Besides promoting grain refinement, large number of HPT cycles maximized the segregation of Li atoms at the α/α boundaries exhibiting lower grain-boundary diffusion than β/β and α/β boundaries (α and β correspond to Mg-rich and Li-rich phases, respectively).[70,71] Such a segregation of Li atoms at the α/α boundaries enhanced its diffusion capability in UFG Mg–8Li alloy. Thus, GBS occurred and high superplastic elongation of 440% was achieved in this alloy even at RT. These results show that decreasing the temperature at which superplasticity is achieved is also possible by enhancing grain-boundary diffusion of difficult to slide boundaries in the microstructure with modification of the chemical composition of these boundaries.

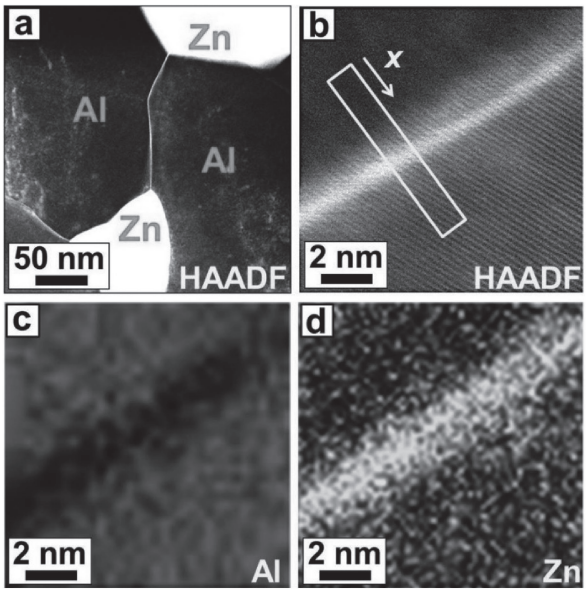


Fig. 9 (a) HAADF images of UFG Al–30Zn alloy after HPT processing. (c)–(d) EDS mapping for Al and Zn atoms obtained from the HAADF image given in (b).[46]

Grain boundary sliding was found to be the main deformation mechanism in all of the studies on RT superplasticity summarized above. Furthermore, GBS was also reported in an HPT-processed Al–Zn alloy showing high ductility and strain rate sensitivity at RT.[72] It is now well established that the deformation mechanism for grain boundary sliding requires the strain rate sensitivity (m) has a value of approximately 0.5 in the conventional superplastic materials to achieve high superplastic elongation.[2] On the other hand, studies on the RT superplasticity of different classes of materials have shown that grain boundary sliding occurs as the main deformation mechanism even though m takes a value of about 0.25 as seen in Table 1. It has been suggested that the low m-value obtained at low temperatures is the result of a threshold stress that must be exceeded so that boundary dislocations escape from the impurity atmosphere and contribute to GBS.[14,73,74] It has been stated that threshold stress resulted from the segregation of impurity atoms at grain boundaries and their interaction with boundary dislocations. Thus, threshold stress is directly related to the diffusivity of the impurity atoms, and decreasing the test temperature increases the threshold stress due to the low diffusion coefficient for grain boundary diffusion at low temperatures.[14,75] Any increase in the threshold stress increases also the flow stress at low strain rates and causes low m-value. Therefore, although GBS occurred as the main deformation mechanism in the alloys exhibited RT superplasticity, low m-values were observed in these alloys due to the relatively low deformation temperature. It is worth to point out that relatively higher m-values of 0.37 and 0.41 were also reported in Refs. 46, 47. As explained above the grain boundary diffusion of Al–30Zn and Mg–8Li alloys were enhanced via HPT. Thus, it is thought that relatively higher m-values were achieved in these alloys despite the low

deformation temperature due to the enhanced grain bonudary diffusion.

4. Summary and Conclusion

Very recent advances in severe plastic deformation (SPD) techniques based on imposing very high strains to the material provide substantial grain refinement and brings about ultrafine-grained (UFG) or nanostructured (NS) microstructural formation in many metals and alloys. Formation of UFG microstructure via SPD methods like equal channel angular pressing (ECAP), high pressure torsion (HPT) and friction stir processing (FSP) bring about a superplastic behavior in some classes of alloys even at room temperature (RT) as an extreme example of low temperature superplasticity. Some experimental data are now available explaining the parameters affecting RT superplasticity in different classes of materials and superplastic deformation mechanisms operated at RT. This paper overviews the available studies aiming to investigate RT superplasticity in some specific UFG metals and alloys after SPD processes, and some conclusions from the investigations are given below.

(1) Equal channel angular pressing (ECAP) and high pressure torsion (HPT) have been successfully utilized for grain refinement to attain UFG microstructure in different classes of metals including Zn–Al, Mg–Li and Al–Zn alloys. Formation of UFG microstructures resulted in excellent superplasticity in these alloys even at RT.

(2) Besides UFG formation, it is shown that decreasing the temperature at which superplasticity is achieved can also be possible by enhancing grain-boundary diffusion of difficult to slide boundaries in the microstructure with modification of the chemical composition of the boundaries.

(3) The available data on RT superplasticity demonstrate that superplastic elongation of severely deformed alloys are controlled by some parameters like size and shape of the grains, homogeneity of the phase distribution throughout the microstructure and chemical composition of the phase/grain boundaries. In general UFG microstructure with homogeneously distributed phases and equiaxed grain morphology were stated to be the optimal parameters for high superplastic elongations at RT. High angle grain boundaries with high diffusivity also promote grain boundary sliding and result in high elongations at RT.

Acknowledgements

This research was supported by Scientific Research Projects of Karadeniz Technical University, Turkey, under Grant no10501. The authors of this study are also grateful to the authors of the reviewed papers for their great studies.

REFERENCES

1) M. Kawasaki and T.G. Langdon: Mater. Sci. **42** (2007) 1782–1796.
2) T.G. Langdon: J. Mater. Sci. **44** (2009) 5998–6010.
3) N. Ridley: *Metals for superplastic forming*, *Superplastic Forming of Advanced Metallic Materials: Methods and Applications*, ed. by G. Giuliano, (Woodhead Publishing Limited, Cambridge, 2011).
4) T.G. Nieh, J. Wadsworth and O.D. Sherby: *Superplasticity in Metals and Ceramics*, first ed., (Cambridge University Press, Cambridge, 1997).
5) K.A. Padmanabhan and G.J. Davies: *Superplasticity, Mechanical and Structural Aspects, Environmental Effects, Fundamentals and Applications*, (Springer-Verlag, Berlin; New York, 1980).
6) T.G. Langdon: Mater. Trans. JIM. **40** (1999) 716–722.
7) S. Komura, Z. Horita, M. Furukawa, M. Nemoto and T.G. Langdon: J. Mater. Res. **15** (2000) 2571–2576.
8) T.G. Langdon: Acta Metall. Mater. **42** (1994) 2437–2443.
9) T. Tanaka, K. Makii, H. Ueda, A. Kushibe, M. Kohzu and K. Higashi: Int. J. Mech. Sci. **45** (2003) 1599–1612.
10) M. Demirtas, G. Purcek, H. Yanar, Z.J. Zhang and Z.F. Zhang: Mater. Sci. Eng. A **644** (2015) 17–24.
11) O.A. Kaibyshev: *Superplasticity of Alloys Intermetallides and Ceramics*, first ed., (Springer-Verlag, New York, 1992).
12) H. Naziri and R. Pearce: Scr. Metall. **3** (1969) 811–814.
13) M. Kawasaki, B. Ahn, P. Kumar, J.-I. Jang and T.G. Langdon: Adv. Eng. Mater. **19** (2017) 1600578.
14) T. Tanaka and K. Higashi: Mater. Trans. **45** (2004) 1261–1265.
15) T. Tanaka, H. Watanabe and K. Higashi: Mater. Trans. **44** (2003) 1891–1894.
16) Y. Huang and T.G. Langdon: J. Mater. Sci. **37** (2002) 4993–4998.
17) C.F. Yang, J.H. Pan and M.C. Chuang: J. Mater. Sci. **43** (2008) 6260–6266.
18) M. Demirtas, H. Yanar and G. Purcek: IOP Conf. Series: Mater. Sci. Eng. **194** (2017) 012033.
19) M. Demirtas, G. Purcek, H. Yanar, Z.J. Zhang and Z.F. Zhang: Mater. Sci. Eng. A **620** (2015) 233–240.
20) S.H. Xia, J. Wang, J.T. Wang and J.Q. Liu: Mater. Sci. Eng. A **493** (2008) 111–115.
21) P. Kumar, C. Xu and T.G. Langdon: Mater. Sci. Eng. A **429** (2006) 324–328.
22) T. Hirata, T. Tanaka, S.W. Chung, Y. Takigawa and K. Higashi: Scr. Mater. **56** (2007) 477–480.
23) M. Demirtas, G. Purcek, H. Yanar, Z.J. Zhang and Z.F. Zhang: J. Alloys Compd. **623** (2015) 213–218.
24) M. Kato, E. Kawai, K. Mutsuzaki and J. Miyagawa: J. Japan Inst. Metals **38** (1974) 539–545.
25) D.H. Shin, J.J. Pak, Y.K. Kim, K.T. Park and Y.S. Kim: Mater. Sci. Eng. A **325** (2002) 31–37.
26) W.H. Huang, C.Y. Yu, P.W. Kao and C.P. Chang: Mater. Sci. Eng. A **366** (2004) 221–228.
27) Y.C. Chen, Y.Y. Huang, C.P. Chang and P.W. Kao: Acta Mater. **51** (2003) 2005–2015.
28) Y.Y. Wang, P.L. Sun, P.W. Kao and C.P. Chang: Scr. Mater. **50** (2004) 613–617.
29) P. Málek, M. Cieslar and R.K. Islamgaliev: J. Alloys Compd. **378** (2004) 237–241.
30) A. Goloborodko, O. Sitdikov, R. Kaibyshev, H. Miura and T. Sakai: Mater. Sci. Eng. A **381** (2004) 121–128.
31) C.P. Chang, P.L. Sun and P.W. Kao: Acta Mater. **48** (2000) 3377–3385.
32) M. Kawasaki, Z. Horita and T.G. Langdon: Mater. Sci. Eng. A **524** (2009) 143–150.
33) S.D. Terhune, D.L. Swisher, K. Oh-ishi, Z. Horita, T.G. Langdon and T.R. McNelley: Metall. Mater. Trans. A **33** (2002) 2173–2184.
34) F.H. Larbi, H. Azzeddine, T. Baudin, M.H. Mathon, F. Brisset, A.L. Helbert, M. Kawasaki, D. Bradai and T.G. Langdon: J. Alloys Compd. **638** (2015) 88–94.
35) R. Valiev: Nat. Mater. **3** (2004) 511–516.
36) C. Xu, Z. Horita and T.G. Langdon: Mater. Sci. Eng. A **528** (2011) 6059–6065.
37) A.P. Zhilyaev, D.L. Swisher, K. Oh-ishi, T.G. Langdon and T.R. McNelley: Mater. Sci. Eng. A **429** (2006) 137–148.
38) R.Z. Valiev, Yu.V. Ivanisenko, E.F. Rauch and B. Baudelet: Acta Mater. **44** (1996) 4705–4712.
39) D.P. DeLo and S.L. Semiatin: Metall. Mater. Trans. A **30** (1999) 2473–2481.

40) Z. Horita, K. Matsubara, K. Makii and T.G. Langdon: Scr. Mater. **47** (2002) 255–260.
41) R.Z. Valiev and T.G. Langdon: Prog. Mater. Sci. **51** (2006) 881–981.
42) T.G. Langdon: Mater. Sci. Eng. A **462** (2007) 3–11.
43) O. Saray and G. Purcek: J. Mater. Process. Technol. **209** (2009) 2488–2498.
44) C.F. Yang, J.H. Pan and T.H. Lee: J. Alloys Compd. **468** (2009) 230–236.
45) M. Demirtas: PhD thesis, Karadeniz Technical University, (2017).
46) K. Edalati, Z. Horita and R.Z. Valiev: Sci. Rep. **8** (2018) 6740.
47) K. Edalati, T. Masuda, M. Arita, M. Furui, X. Sauvage, Z. Horita and R.Z. Valiev: Sci. Rep. **7** (2017) 2662.
48) T.G. Langdon: Mater. Sci. Eng. A **174** (1994) 225–230.
49) Y.H. Zhao, Y.Z. Guo, Q. Wei, A.M. Dangelewicz, C. Xu, Y.T. Zhu, T.G. Langdon, Y.Z. Zhou and E.J. Lavernia: Scr. Mater. **59** (2008) 627–630.
50) Y.H. Zhao, Y.Z. Guo, Q. Wei, T.D. Topping, A.M. Dangelewicz, Y.T. Zhu, T.G. Langdon and E.J. Lavernia: Mater. Sci. Eng. A **525** (2009) 68–77.
51) M. Demirtas, G. Purcek, H. Yanar, Z.J. Zhang and Z.F. Zhang: J. Alloys Compd. **663** (2016) 775–783.
52) T. Tanaka and K. Higashi: Mater. Trans. **45** (2004) 2547–2551.
53) M. Kawasaki and T.G. Langdon: Mater. Trans. **53** (2012) 87–95.
54) C. Xu, M. Furukawa, Z. Horita and T.G. Langdon: Adv. Eng. Mater. **5** (2003) 359–364.
55) M. Kawasaki, C. Xu and T.G. Langdon: Acta Mater. **53** (2005) 5353–5364.
56) R.B. Figueiredo and T.G. Langdon: Mater. Sci. Eng. A **556** (2012) 211–220.
57) T. Hirata, T. Mukai, N. Saito, S. Tanabe, M. Kohzu and K. Higashi: J. Mater. Sci. **38** (2003) 3925–3932.
58) T. Hirata, T. Osa, H. Hosokawa and K. Higashi: Mater. Trans. **43** (2002) 2385–2391.
59) T. Watanabe: Mater. Sci. Eng. A **166** (1993) 11–28.
60) H. Kokawa, T. Watanabe and S. Karashima: Philos. Mag. A **44** (1981) 1239–1254.
61) I.C. Choi, Y.J. Kim, B. Ahn, M. Kawasaki, T.G. Langdon and J. Jang: Scr. Mater. **75** (2014) 102–105.
62) M. Furukawa, Y. Ma, Z. Horita, M. Nemoto, R.Z. Valiev and T.G. Langdon: Mater. Sci. Eng. A **241** (1998) 122–128.
63) P. Shariat, R.B. Vastava and T.G. Langdon: Acta Metall. **30** (1982) 285–296.
64) P. Kumar, C. Xu and T.G. Langdon: Mater. Sci. Eng. A **410–411** (2005) 447–450.
65) H. Naziri, R. Pearce, M.R. Brown and K.F. Hale: Acta Metall. **23** (1975) 489–496.
66) I.I. Novikov, V.K. Portnoy and T.E. Terentieva: Acta Metall. **25** (1977) 1139–1149.
67) A. Alhamidi, K. Edalati, Z. Horita, S. Hirosawa, K. Matsuda and D. Terad: Mater. Sci. Eng. A **610** (2014) 17–27.
68) R.Z. Valiev, M.Y. Murashkin, A. Kilmametov, B. Straumal, N.Q. Chinh and T.G. Langdon: J. Mater. Sci. **45** (2010) 4718–4724.
69) B.B. Straumal, B. Baretzky, A.A. Mazilkin, F. Phillipp, O.A. Kogtenkova, M.N. Volkov and R.Z. Valiev: Acta Mater. **52** (2004) 4469–4478.
70) H. Mehrer: *Numerical Data and Functional Relationship in Science and Technology*, *Diffusion in Solid Metals and Alloys*, Vol. 26, (Springer, Berlin, 1990).
71) G. Langen, G. Schwitzgebel and H. Ruppersberg: Mater. Res. Bull. **19** (1984) 1141–1147.
72) N.Q. Chinh, R.Z. Valiev, X. Sauvage, G. Varga, K. Havancsak, M. Kawasaki, B.B. Straumal and T.G. Langdon: Adv. Eng. Mater. **16** (2014) 1000–1009.
73) T. Uesugi, M. Kawasaki, M. Ninomiya, Y. Kamiya, Y. Takigawa and K. Higashi: Mater. Sci. Eng. A **645** (2015) 47–56.
74) F.A. Mohamed: Mater. **4** (2011) 1194–1223.
75) F.A. Mohamed: J. Mater. Sci. **18** (1983) 582–592.